energies

MDPI

Article

Planetary Gear-Enhanced Electromagnetic and Triboelectric Self-Powered Sensing System for Corn Seeders

Longgang Ma †, Han Wu †, Maoyuan Yin, Zhencan Yang, Dong Wang, Ruihua Zhang and Xinqing Xiao *

College of Engineering, China Agricultural University, Beijing 100083, China
* Correspondence: xxqjd@cau.edu.cn
† These authors contributed equally to this work.

Abstract

In response to issues such as traditional monitoring devices relying on external power sources and poor environmental adaptability during corn sowing, this paper designs a composite self-powered sensing system (EPTG) based on a planetary gear system coupled with a triboelectric nanogenerator (P-TENG) and an electromagnetic generator (EMG). The system utilizes the speed-increasing characteristics of planetary gear systems and flexibly designs gear teeth to adapt to different working conditions, achieving multiple transmission ratio combinations to provide stable power input for composite power generation units and improving mechanical energy capture and conversion efficiency. Under typical operating conditions (with the seeder operating at an average speed of 25 rpm), the EPTG can consistently deliver 105 mW of power. Combined with low-power program design and a 900 mAh energy storage battery, it can reliably power the monitoring unit equipped with integrated infrared sensors and temperature/humidity sensors, enabling the system to operate on self-generated power. Monitoring data is wirelessly transmitted to a cloud platform for visualization and analysis, providing decision support for precise seeding. Experimental results show that EPTG operates stably with good durability. It provides a practical solution for energy self-sufficiency and operational precision in agricultural intelligent equipment, and may have application value in related areas.

Keywords: planetary gear system; TENG; self-powered sensing system; corn seeder

check for updates

Academic Editor: Daniel Morinigo-Sotelo

Received: 9 July 2025
Revised: 27 July 2025
Accepted: 6 August 2025
Published: 8 August 2025

Citation: Ma, L.; Wu, H.; Yin, M.; Yang, Z.; Wang, D.; Zhang, R.; Xiao, X. Planetary Gear-Enhanced Electromagnetic and Triboelectric Self-Powered Sensing System for Corn Seeders. *Energies* **2025**, *18*, 4236. https://doi.org/10.3390/en18164236

Copyright: © 2025 by the authors. Licensee MDPI, Basel, Switzerland. This article is an open access article distributed under the terms and conditions of the Creative Commons Attribution (CC BY) license (https://creativecommons.org/licenses/by/4.0/).

1. Introduction

As one of the most widely distributed staple crops in the world, corn cultivation directly affects the food security of one-third of the global population [1–3]. In the corn production chain, quality control during the sowing stage is particularly critical, as its effectiveness directly determines subsequent germination rates and final yields. Currently, seed skipping remains a prominent issue affecting sowing quality. This not only leads to gaps in the field and increased costs for subsequent operations such as reseeding, but also significantly reduces total corn yields [4]. Therefore, real-time, accurate monitoring of the operating status of seeders has become a core requirement for improving corn seeding technology. The key prerequisite for achieving this goal is to equip seeders with stable and reliable monitoring devices. Among these, self-powered devices, which can break free from the limitations of traditional power supply methods and adapt to complex field environments, have become an important technological breakthrough in solving the problem of real-time monitoring of seeding status [5].

With the in-depth promotion of smart agriculture and sustainable development concepts, the application of environmental energy harvesting technology in the field of agricultural equipment has attracted widespread attention [6]. Among them, triboelectric nanogenerators (TENG) are a new type of energy conversion device based on the triboelectric effect and electrostatic induction effect. They demonstrate high efficiency in converting environmental mechanical energy, and can convert dispersed mechanical energy such as tree branch vibrations [7], human movement [8,9], and wind energy [10] into electrical energy. Since Zhonglin Wang first proposed this technology in 2012 [11], it has achieved breakthrough applications in many fields. For example, Fang Yi et al. used stretchable rubber materials to construct a triboelectric generator that can accurately monitor human movements [12], and Jin et al. integrated TENG into bionic fingers to achieve real-time motion state collection [13]. However, TENG still has significant limitations in agricultural equipment applications. Its output current is relatively small, and it performs poorly in terms of high-frequency response and long-term stability, making it difficult to meet the continuous monitoring requirements of equipment such as seeders [14].

In contrast, electromagnetic power generation technology (EMG) operates based on Faraday's law of electromagnetic induction and, thanks to its high stability in collecting mechanical energy at medium to high frequencies, has been widely applied in everyday life and industrial settings. The alternating magnet arrangement generator designed by Li et al. can charge a 10 μF capacitor to approximately 0.68 V within 400 s, significantly outperforming the energy storage efficiency of the Halbach arrangement (0.51 V) and the separated arrangement (0.38 V) [15]. Zhang et al. developed a wind power generation device that successfully provides stable power to IoT nodes and wind speed sensors [16], while Zhao et al. proposed a tidal energy WEC device that has completed field testing for wave power generation [17]. However, EMG also has notable shortcomings, as it has low sensitivity to low-speed mechanical movements, making it difficult to capture the low-frequency, intermittent mechanical energy commonly found in seeder operations, resulting in inadequate energy utilization [18,19].

To overcome the limitations of single power generation technologies, the Triboelectric–Electromagnetic Hybrid Generator (TEHG) was developed. This technology integrates the operational mechanisms of TENG and EMG, leveraging their complementary characteristics in terms of operating frequency ranges and energy harvesting properties. TENG excels at capturing low-frequency, intermittent friction energy, while EMG demonstrates superior efficiency in high-frequency rotational energy conversion. This enables the efficient utilization of mechanical energy across the entire frequency spectrum, making it a current research hotspot in the field of energy harvesting [20]. For example, Lee's Slinky spring-structured hybrid generator can generate a peak voltage of 8.837 V and a current of 49.6 mA by manual shaking, successfully driving multiple LEDs and charging a capacitor [21]; Zeeshan et al. developed a thermomagnetically driven TEHG that achieves a maximum output power of 0.75 mW under conditions of a 45 °C temperature difference and 251 rpm rotational speed, demonstrating excellent low-temperature-difference energy conversion efficiency [22]; and Bjelica et al. combined one TENG with two EMGs to construct a hybrid nanogenerator that achieved a maximum output voltage of 65.131 V and a current of 15.25 μA, capable of driving at least 94 series-connected LEDs or 50 parallel-connected LEDs [23]. It is worth noting that while wireless power transmission technology offers application advantages in specific scenarios due to its lack of physical wiring, its applicability in agricultural field environments is limited: on the one hand, the core components and deployment costs of this technology conflict with the low-cost requirements of agricultural sensing systems; on the other hand, the open nature of agricultural fields and the dispersed nature of operational areas can easily cause signal interference, leading to insufficient transmission stability and

making it difficult to meet continuous monitoring requirements [24]. In contrast, TEHG, by integrating the complementary characteristics of TENG and EMG, better aligns with the cost and stability requirements for energy harvesting devices in agricultural scenarios. The aforementioned research indicates that TEHG possesses significant application potential in complex mechanical energy environments, offering a new approach to addressing the self-powering challenges of agricultural equipment such as seeders.

Based on the above background, this study proposes a composite self-powered sensing system for corn seeding machinery using an integrated planetary gear system. This system combines a friction nanogenerator (P-TENG) and an electromagnetic generator (EMG) based on the planetary gear system (EPTG). EPTG leverages the speed-increasing characteristics of the planetary gear system in low-speed seeding environments, combined with a flexible tooth count design to adapt to different operational conditions, enabling multiple gear ratio combinations. This provides stable power input to the composite power generation unit, significantly enhancing the capture and conversion efficiency of mechanical energy. Under typical operating conditions (average seeding machine speed of 25 rpm), the EPTG stably outputs 105 mW of power. Combined with low-power design and a 900 mAh energy storage battery, it ensures a stable, self-sufficient energy supply. The sensing system integrates infrared photoelectric sensors (IR sensors) and temperature and humidity sensors (TH sensors) to monitor relevant parameters during the seeding process. Additionally, low-power program design significantly reduces the system's average energy consumption, forming an efficient collaboration with the composite power generation unit. The collected seeding data is transmitted wirelessly to the cloud platform, where it undergoes visualization analysis, providing timely and reliable decision support for precise seeding. This integrated approach, combining composite energy harvesting, multi-parameter sensing, low-power design, wireless transmission, and cloud-based analysis, not only enables the system to operate with self-sufficient energy but also enhances the intelligence and precision of corn seeding monitoring.

2. Materials and Methods

2.1. System Architecture

Addressing technical challenges in corn seeding operations, such as sensors relying on an external power supply and insufficient environmental adaptability, this study proposes a self-powered sensing system based on a coupled power generation mechanism combining a planetary gear-based triboelectric nanogenerator (P-TENG) and an electromagnetic generator (EMG). This system innovatively converts the kinetic energy generated during the movement of the seeding machinery into electrical energy, establishing an integrated solution for energy harvesting, storage, and low-energy consumption. This innovation partially alleviates the power supply and environmental adaptability issues of traditional sensing systems, providing new insights for energy autonomy and operational precision in agricultural intelligent equipment, and holds significant application potential [25].

As shown in Figure 1a, the system uses the mechanical motion of the seeding machine as an energy input source. As shown in Figure 1b, the sensor module integrates an IR sensor and a TH sensor, which can monitor environmental temperature and humidity parameters and seeding density data in real time, providing key decision-making information for precision corn seeding. The system adopts a modular design (Figure 1c), consisting of a self-powered module, a power management module, a sensor module, and an upper-level computer module. The self-powered module utilizes a TENG and EMG working in tandem through a planetary gear system to efficiently capture mechanical energy and convert it into electrical energy. The power management module is responsible for rectifying, regulating, and storing the collected electrical energy; the sensor module includes an IR sensor, a TH

sensor, and a microcontroller unit (MCU), supporting real-time data collection and wireless transmission; and the host computer module (Figure 1d) is based on cloud platform technology, enabling real-time reception, visualization analysis, and intelligent decision-making of seeding data (including geographical location, environmental parameters, seeding density, and sensor online status).

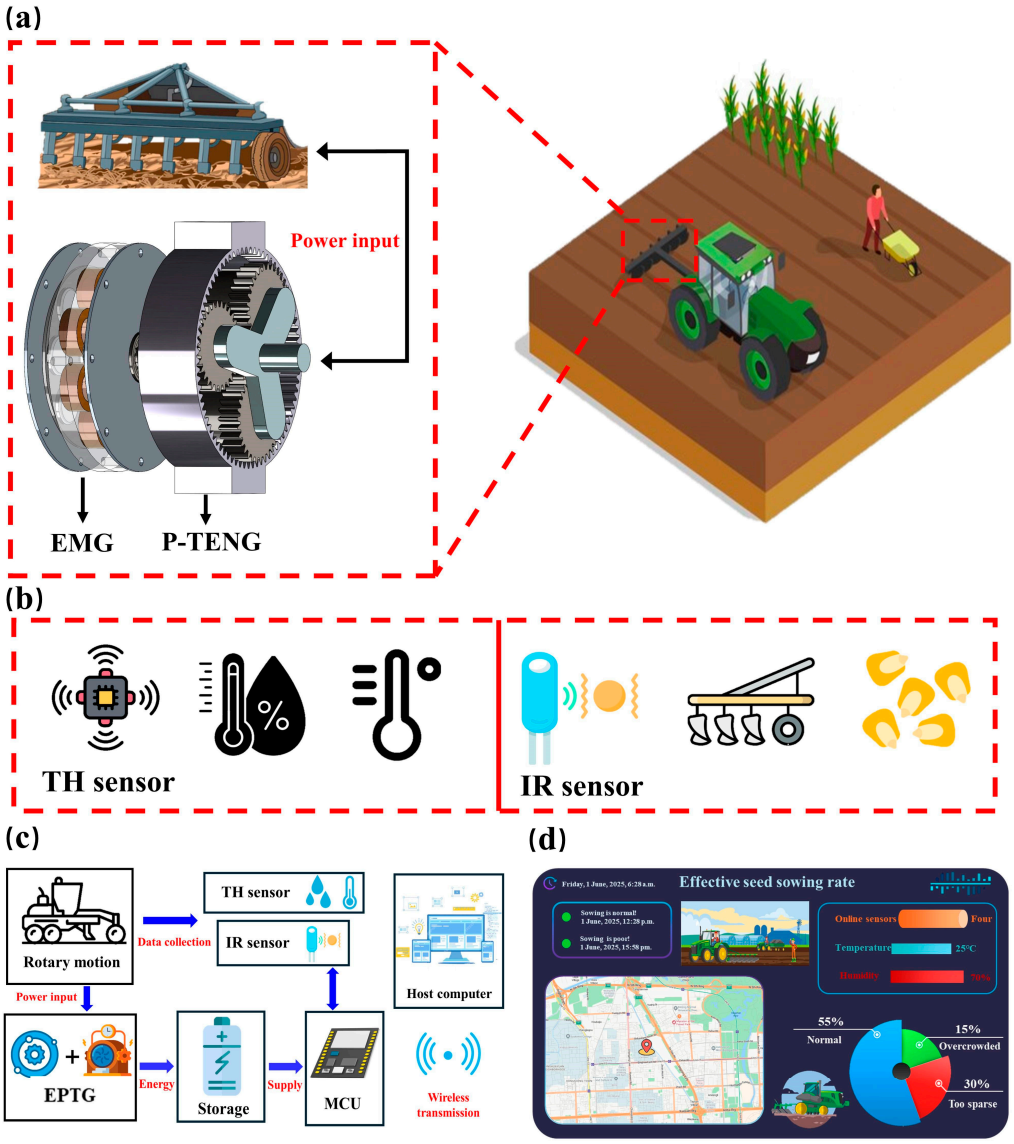


Figure 1. Overall system architecture: (**a**) Field conditions for corn seeders and EPTG layout. (**b**) TH sensors and IR sensors used in the sensing system. (**c**) Structure of the various parts of the system. (**d**) Visualization of sowing data on the host computer cloud platform.

This self-powered sensing system effectively alleviates the limitations of traditional power supply modes through the deep integration of composite power generation technology and intelligent sensing technology, significantly improving the applicability of equipment in complex farmland environments. It provides reliable technical support for the intelligent monitoring and precise control of corn sowing operations, promoting the transformation and upgrading of agricultural production towards intelligence and efficiency.

2.2. EPTG Implementation

To address the power supply challenges faced by agricultural IoT devices in open farmland environments, this study developed a multi-modal energy harvesting architecture. By integrating variable-speed transmission and composite power generation devices into seeders, the architecture enables efficient conversion of mechanical kinetic energy into electrical energy, providing an innovative technical solution for addressing the issue of sustained power supply for field devices. The study proposes a composite power supply device (EPTG), which combines a planetary gear transmission mechanism with a TENG and an EMG. As shown in Figure 2a, the core component of the EPTG, the EMG, adopts a modular design. Its mechanical structure consists of a stator and a rotor. The stator comprises eight copper coils with a diameter of 15 mm, which are fixed to a resin rubber substrate via an embedding process and covered with insulating material to ensure coil positioning accuracy and electrical safety. The rotor is composed of two layers of aluminum plates, with eight permanent magnets evenly distributed around the circumference of each aluminum plate. The adjacent magnetic poles are spaced at 45° angles and are rigidly connected to the rotating shaft via high-strength bolts, forming a stable rotating unit. The EMG spindle and the sun gear of the planetary gear system are assembled using a coaxial nested configuration, enabling seamless power coupling and transmission. This structural design is based on the principle of electromagnetic induction, generating induced currents through the relative motion between the stator coils and the rotor permanent magnets. Additionally, the axially symmetric layout effectively suppresses vibrations during operation, ensuring system stability.

The mechanical system of the friction nanogenerator (P-TENG), based on a planetary gear transmission, consists of a planetary gear transmission mechanism and a TENG energy conversion unit. Its mechanical structure is shown in Figure 2a, comprising a ring gear, sun gear, planetary gears, and planetary carrier, as well as a friction layer, dielectric layer, and interdigitated electrodes. Among these, the ring gear serves as the stator and is fixed in place, while the remaining components form the rotor system. The seeder's power input drives the planetary carrier, causing the planetary gears to move; the relative displacement between the planetary gears and the toothless sections of the ring gear forms the basis for energy conversion. Specifically, the toothless regions of the planetary gears are equipped with copper friction layers, while the toothless regions of the ring gear integrate finger electrodes and are covered with a dielectric layer, together forming the friction nanogenerator unit. Considering the low-speed operating conditions of corn seeders, the planetary gear system is used as a speed-increasing mechanism, with the number of teeth on each component of the planetary gear system designed flexibly according to the actual rotational speed of the seeder. In this study, standard gears were selected, with the number of teeth on the ring gear, planetary gears, and sun gear set to 140, 60, and 20, respectively. In terms of electrode preparation, as shown in Figure 2b, the interdigitated electrodes were fabricated using ultraviolet nanosecond laser processing technology, etched onto a copper-clad polyimide (PI) substrate; as shown in Figure 2c, the formed electrode surface was uniformly coated with a polytetrafluoroethylene (PTFE) dielectric layer. During operation, the copper foil friction layer of the planetary gear experiences relative friction with the PTFE dielectric layer. Through the coupled effects of triboelectric charging and electrostatic induction, mechanical energy is efficiently converted into electrical energy. Additionally, as shown in Figure 2d, the interdigital electrode electrodes are formed into long strip-shaped electrode strips through multi-segment composite processing and precisely adhered to the inner side of the gear ring. All components of the planetary gear system are integrally formed using 3D printing technology, ensuring structural precision and assembly reliability.

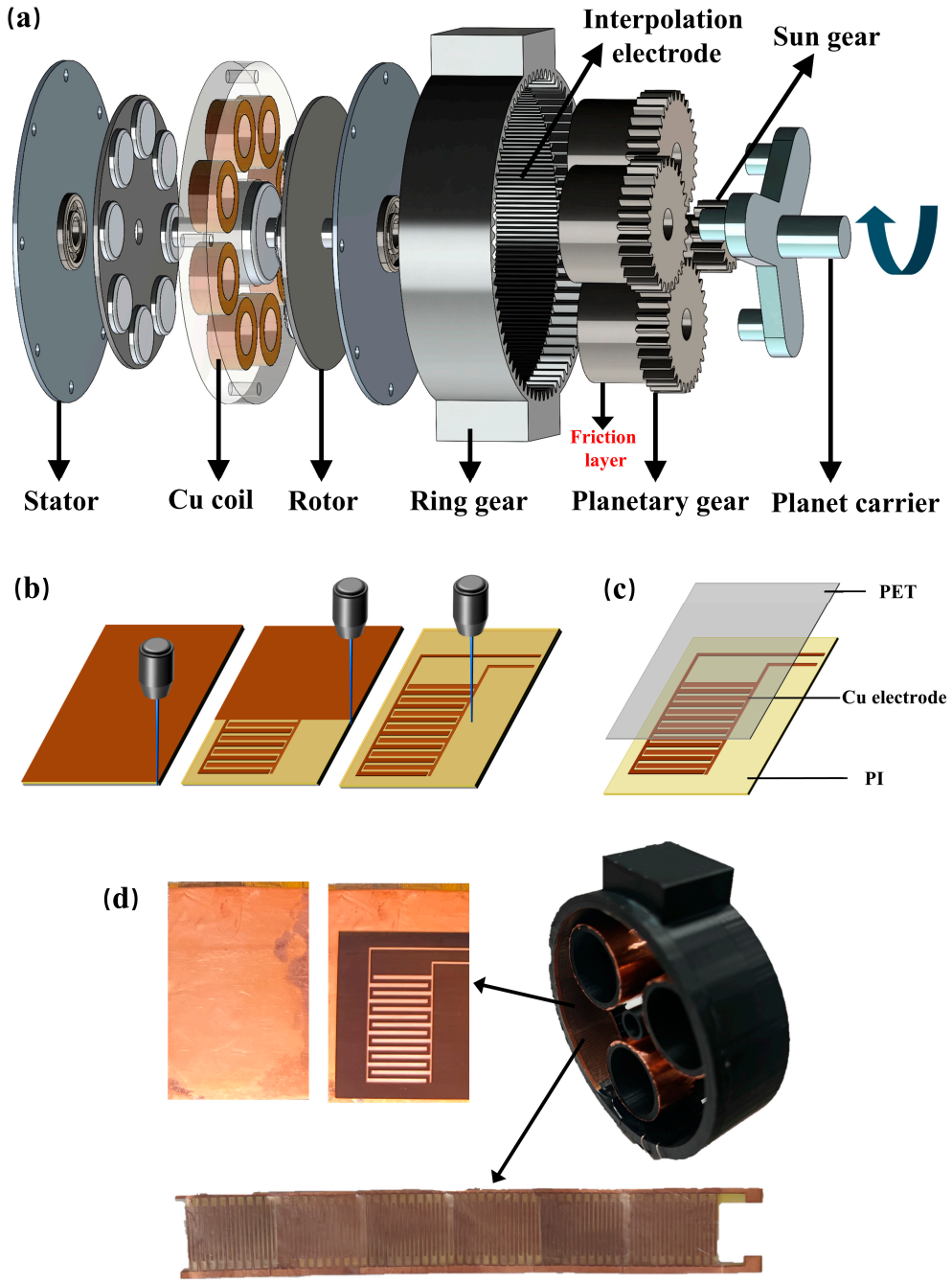


Figure 2. Structure and physical diagram of EPTG: (**a**) Exploded view of EPTG. (**b**) Fabrication of interpolation electrodes. (**c**) Interpolation electrode materials of different layers. (**d**) Assembly drawing of EPTG.

Additionally, based on institutional kinematics theory, for a 2K-H type planetary gear transmission system, a transmission ratio mathematical model can be constructed under specific constraint conditions. Specifically, when the planetary carrier serves as the driven component for power input, the ring gear is in a fixed constrained state, and the sun gear is mechanically coupled to an electromagnetic generator; the transmission ratio mathematical expression of the transmission system can be derived by adjusting the gear tooth ratio and combining it with the basic kinematic equations of the planetary gear mechanism. This clarifies the speed conversion relationship and provides a theoretical foundation for subsequent analysis of energy harvesting efficiency [26–28]. In this paper, the number of

teeth for the ring gear, planetary gears, and sun gear is 140, 60, and 20, respectively. Based on the principle of gear meshing, the transmission ratio formula is as follows:

$$n_1 z_1 + n_3 z_3 = n_H (z_1 + z_3) \quad (1)$$

$$n_2 = n_H + \frac{z_1}{z_2}(n_H - n_1) \quad (2)$$

where n_1, n_2, n_3, and n_H represent the rotational speeds of the sun gear, planetary gears, ring gear, and planetary carrier, respectively. The rotational speed of the planetary carrier is its self-rotation speed, and its orbital rotational speed is equal to that of the planetary carrier.z_1, z_2, and z_3 represent the number of teeth on the sun gear, planetary gears, and ring gear, respectively.

By reasonably designing the gear tooth ratio, the rotational speeds of the sun gear and planetary gears can be effectively controlled, thereby providing a stable rotational speed input for the EPTG to achieve maximum power output.

2.3. Experimental Scheme

This experiment uses 75 μm thick polyimide (PI), polyethylene terephthalate (PET), and polytetrafluoroethylene (PTFE) films as dielectric layers, 100 μm thick copper foil as the friction layer, and 150 μm thick copper-clad laminate as the electrode conductive substrate. The interdigitated electrode pattern was precisely etched using a UV nanosecond laser (UV-Jianshi, Tianjin Meiman Laser Technology Co., Ltd. Tianjin, China) at 90% power and a speed of 100 mm/s; all gear components were manufactured as a single piece using a Chuangxiang K1Max 3D printer (Shenzhen, China). Sensor power consumption performance was conducted using an electrochemical workstation, and ETPG electrical performance parameters were obtained through multiple repeated measurements using a Keithley 6514(Ohio, United States) electrometer. Environmental temperature and humidity monitoring uses the SHT30 (Stafa, Switzerland) sensor (temperature range −40 °C to 80 °C, humidity accuracy ±3% RH), seed fall detection uses the E18-D80NK (Zhe jiang China) infrared photoelectric sensor, and the control unit uses the eps32 microcontroller.

(1) COMSOL 6.1 simulation based on EMG and P-TENG principles

This study aims to utilize the COMSOL 6.1 Multiphysics simulation platform to establish a coupled energy harvesting system model integrating an electromagnetic generator (EMG) and a friction nanogenerator (P-TENG). Through material parameterization design (EMG: copper coils and NdFeB permanent magnets; P-TENG: PTFE dielectric film and copper metal electrodes), under uniform mechanical excitation conditions, to systematically analyze the output characteristics and energy conversion efficiency of different material combinations. This will validate the feasibility and synergistic working mechanism of the hybrid energy harvesting scheme, providing a theoretical basis for subsequent experimental design and device optimization.

(2) EPTG performance

This experiment utilizes a self-built controllable speed test platform to investigate the electrical output characteristics of EPTG. The platform has a speed adjustment range of 30–500 rpm, with a control accuracy of ±5 rpm. It integrates a planetary gear speed change mechanism, enabling efficient and stable speed control and wide-range output, providing precise and controllable power input conditions for the experiment. The experiment employs the Keithley 6514 high-precision electrical signal measurement instrument to simultaneously collect the open-circuit voltage (Voc) and short-circuit current (Isc) of the EPTG under different speed conditions. Based on the principle of maximum power transfer, the generator's peak power output under optimal operating conditions is determined

through load matching optimization, comprehensively characterizing its power generation performance.

In terms of material research, three typical dielectric materials, PTFE, PET, and PI, were selected to construct the friction layer, with an in-depth investigation into the mechanisms by which material properties influence generator performance. A systematic comparative analysis of the dielectric properties, surface charge storage characteristics, and long-term stability of each material is conducted. Combined with generator output voltage, current, and power data, the friction layer material with the optimal performance is selected. Additionally, specialized experiments are conducted on the P-TENG module to study the correlation between its output voltage and rotational speed, as well as material parameters, providing a detailed theoretical basis and data support for material selection and structural optimization of EPTG devices.

(3) System application performance

This study employs multi-dimensional systematic performance to investigate the comprehensive performance of the EPTG power supply system in real-world application scenarios. During the experiment, a power analyzer is used to simulate energy input conditions under varying environmental conditions, enabling dynamic monitoring and quantitative analysis of the EPTG's real-time output power and sensing system power consumption. This allows for an exploration of the system's energy consumption characteristics under complex operating conditions, thereby verifying its compliance with energy consumption standards in practical applications. In a simulated field corn seeding application scenario within an agricultural machinery laboratory, IR sensors and TH sensors were used to collect real-time data on seed fall and environmental temperature and humidity, and to precisely calculate seed fall density, seeding spacing, and other data. This enabled an assessment of the accuracy and reliability of sensor data collection under EPTG power supply conditions, ensuring the validity and scientific rigor of the monitoring data in real-world applications.

For the durability assessment of EPTG, it was deployed on an adjustable speed experimental test platform to conduct long-term, continuous operation tests. Key performance parameters such as output voltage, current, and power were recorded to track their degradation trends, thereby systematically evaluating the stability and reliability of the device during long-term operation. This provides data support for predicting the service life of the device in actual application scenarios. For the performance of wireless data transmission in the sensing system, this experiment deployed WIFI modules to establish transmission links based on variations in agricultural machinery density and communication distances. Typical environments such as open farmland and areas with dense agricultural machinery operations were selected to monitor metrics such as data upload success rates and packet loss rates. The stability of transmission under different distances and interference intensities was verified. Considering that actual farmland interference is weaker than in experimental scenarios, the impact of signal interference on communication quality and effective transmission distance was analyzed. The experiment evaluates the system's adaptability and robustness in actual seeding environments, providing support for the practical verification of the EPTG power supply system.

3. Results and Discussion

3.1. Operation Principle of EMG and P-TENG

The EMG energy harvesting system is based on Faraday's law of electromagnetic induction. Faraday's law of electromagnetic induction can be expressed in Formula (3). It drives the permanent magnet rotor to rotate through the rigid coupling between the sun

gear and the shaft in the planetary gear system, causing the magnetic flux in the copper coil to change periodically with the angular displacement of the rotor, thereby generating an alternating induced electromotive force in the coil [29,30]. As shown in Figure 3a, in the relative motion of the permanent magnet and the coil, when the magnet and the coil axis are relatively far away from each other, the magnetic flux through the coil exists, but the rate of change is almost zero, so there is no induced current in the coil (1). With the beginning of the rotation of the rotor, the distance between the magnet and the coil gradually becomes smaller and smaller, the angle between the two continues to narrow, and the magnetic flux through the coil shows an exponential upward trend. The magnetic flux through the coil increases exponentially, and this process of magnetic flux increase stimulates a positive induced current in the coil (2). When the direction of the magnetic poles completely coincides with the coil axis, the magnetic flux reaches the maximum value in the whole cycle, but because the whole coil is equivalent to the cutting of magnetic inductance in the constant magnetic field, the rate of change in magnetic flux is zero, so it does not produce induced currents (3). The rotor continues to rotate so that the magnetic poles gradually deviate from the coil axis and the magnetic flux. With the exponential decline, the coil will be induced in the opposite direction of the current (4), until the coil is gradually away from the magnetic poles, the rate of change in magnetic flux drops abruptly, back to the initial state, the induced current also disappeared, and thus a complete cycle of electromagnetic induction is completed.

$$\varepsilon = -N\frac{d\varnothing}{dt} \tag{3}$$

where ε is the induced electromotive force, $\frac{d\varnothing}{dt}$ is the rate of change in magnetic flux with time, and N is the number of turns of the induction coil. As the conductor loop moves through the magnetic field, the magnetic flux $\varnothing$ changes, resulting in an induced electromotive force. When the kinetic energy generated by the corn seeder drives the magnet-equipped rotor to rotate in one direction, it periodically alters the magnetic flux in the Cu coil in the EMG, inducing an electromotive force and generating a periodic alternating current.

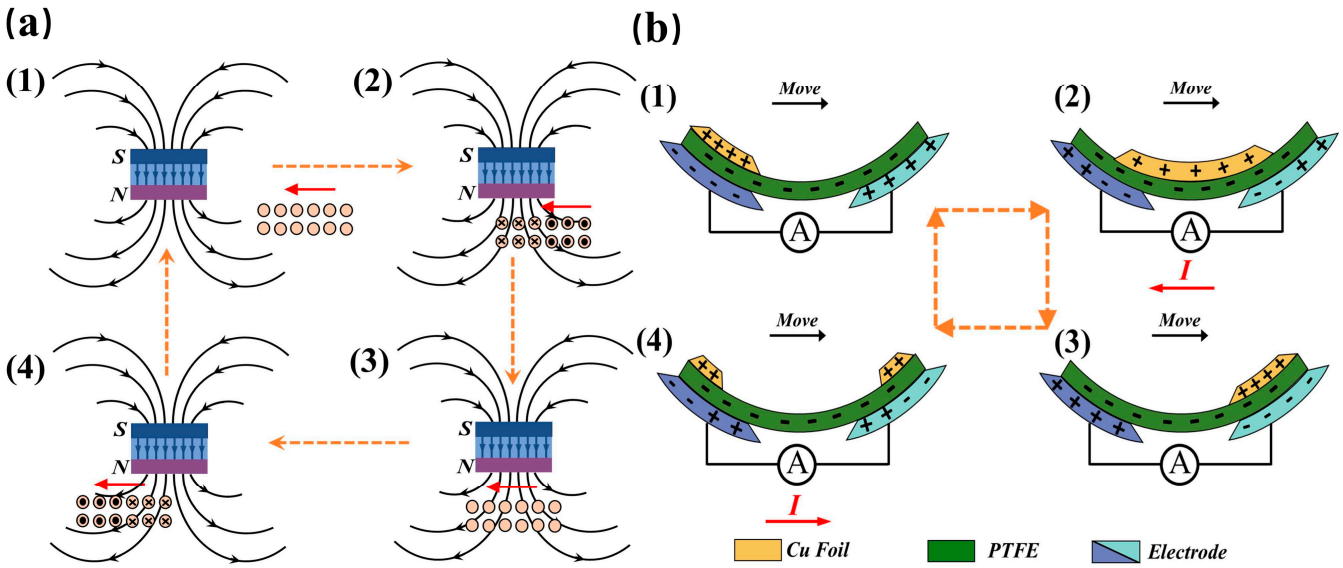


Figure 3. Working mechanism of EMG and P-TENG: (**a**) Magnetic flux line distribution of EMG and direction of coil induction current in four typical situations. (**b**) Potential distribution of P-TENG in four different positions.

The operating mechanism of P-TENG follows the independent layer mode of TENG. Its core principle stems from the contact electret and electrostatic induction coupling effects caused by the difference in electronegativity between different materials: when two material layers undergo relative motion during contact separation, electrons transfer due to differences in surface electron affinity energy, thereby forming an electrostatic charge distribution at the interface. During separation, the charge imbalance drives charge carriers to migrate through the external circuit, generating measurable current and voltage outputs [31,32]. Taking the copper foil and PTFE dielectric friction layer system as an example, the power generation process is essentially a physical process of charge transfer induced by the difference in electron affinity between copper and PTFE. In this study, when the planetary gear's toothless section is stationary in the initial state, no contact occurs at the friction interface, and the charge transfer process remains dormant. When the planetary carrier drives the planetary gear to rotate, the copper foil attached to the gear surface moves sequentially across the PTFE dielectric layer on the surface of the interdigitated electrodes as the mechanism moves. Due to the inherent differences in electron gain/loss capabilities between PTFE and copper foil, electrons migrate directionally from the copper foil surface to the PTFE surface upon contact, causing PTFE to accumulate negative charges while the copper foil becomes positively charged [33]. This charge separation state forms a periodic cycle of charge induction and release as the gear rotates, manifesting as a regular current output characteristic in the external circuit.

In essence, the theoretical foundation of TENG lies in the Maxwell displacement current. By transforming the differential form of the Maxwell–Ampere law equations, we obtain Formula (4).

$$J_D = \frac{\partial D}{\partial t} = \varepsilon \frac{\partial E}{\partial t} + \frac{\partial P_s}{\partial t} \tag{4}$$

where J_D is the Maxwell displacement current density, D is the potential shift vector, ε is the dielectric constant of the dielectric, E is the electric field strength, and P_s is the polarization field density. $\frac{\partial P_s}{\partial t}$ is the current induced by the polarization field generated by the electrostatic charge carried by the surface, which is the fundamental theoretical basis and source of TENG. In fact, the actual mathematical model of TENG involves more complex factors such as additional parameters, nonlinear effects, and different friction material properties. The basic principles presented here provide a foundation for understanding TENG and its practical applications.

As shown in Figure 3b, during the rotation of the copper foil in the direction of the planetary gear, in the initial state when the copper foil is in contact with the left electrode (1), the negative charges in the circuit are directed to collect in the corresponding contact area of this electrode by electrostatic interactions. As the copper foil rotates and comes into contact with the right electrode (2), the negative charge migrates to the newly contacted right electrode with the help of the load circuit, thus forming a current directed to the left. When the copper foil completely covers the right electrode (3), the potential difference between the two electrodes tends to disappear due to the dynamic equilibrium of the charge distribution, and the directional flow of charge is then stagnant. When the copper foil continues to rotate and comes into contact with the left electrode again (4), the negative charge, driven by the electrostatic induction effect, flows back to the initially contacted left electrode area through the load circuit, generating a current in the right direction. This cycle realizes the cyclic transfer process of negative charge between different electrodes. It is worth noting that the negative charge on the surface of PTFE in a stationary state can neither change the intrinsic induced potential distribution between the electrodes nor provide power support for the directional movement of the charge. It can be seen that the rotational behavior of the positively charged copper foil is the core driving force

that triggers the directional transfer of charge and contributes to the formation of current, which plays a key role in the initial process of electrical energy generation in P-TENG. The COMSOL 6.1 simulation results of the corresponding states have been analyzed in detail by Wu et al. [33,34].

Additionally, to address the application requirements of the P-TENG adapter gear ring's narrow inner diameter space, a rolling structure with interdigitated electrodes arranged along the inner wall of the gear ring was adopted to replace the traditional planar sliding design. Although the reduced contact area decreases the induced charge quantity, the interdigitated structure completes the power generation cycle through single-grid displacement, thereby enhancing the electronic reciprocating frequency and charge transfer efficiency [35,36]. Furthermore, by establishing an adjustable correlation between the copper foil sweeping speed and the planetary carrier rotational speed based on tooth count parameters, the relative speed is precisely matched to achieve maximum power generation. By synergistically regulating the charge transfer cycle through the coordination of planetary gear tooth count and rotational speed, combined with the synergistic effect of multiple electrodes, power generation performance is significantly enhanced, making it an optimal solution for power generation in confined spaces [37,38].

3.2. EMG and P-TENG Performance

To investigate the power generation performance of P-TENG driven by the rotational motion of a seeding machine, the experiment used a high-sampling-frequency electrometer to collect real-time voltage and current signals. A stepper motor with adjustable speeds ranging from 30 rpm to 500 rpm was used to drive the planetary frame, simulating the performance of a seeding machine under different operating conditions. As shown in the experimental data in Figure 4a,b, when the stepper motor speed is fixed at 300 rpm, the dielectric material significantly affects the power generation performance of the P-TENG. When PET and PI are used as the dielectric layer, the open-circuit voltage of the P-TENG reaches 2.8 V and 3.9 V, respectively, with short-circuit currents of 153 nA and 124 nA, respectively. However, when PTFE was used as the dielectric layer, the open-circuit voltage of the TENG increased to 8.6 V, and the short-circuit current rose to 224 nA, demonstrating superior power generation performance and providing data support for the application of this structure in real-world scenarios. The above study clarified the mechanism by which dielectric materials influence the power generation performance of P-TENG. However, in the actual operation of seeding machinery, the planetary frame speed undergoes dynamic changes. Therefore, investigating the power generation characteristics of P-TENG within the speed range of 30 rpm to 500 rpm and quantifying the relationship between speed and electrical output is of significant importance for enhancing its operational adaptability and energy conversion efficiency.

As shown in the experimental data in Figure 4c,d, when the rotational speed of the P-TENG friction layer varies between 50 rpm and 500 rpm, the peak Isc increases significantly from 61 nA to 532 nA as the rotor speed increases, while Voc remains stable at around 8.5 V. This phenomenon fundamentally stems from the characteristic differences between Voc and the short-circuit current Isc. Voc depends on the maximum overlap area between the PTFE film and the copper finger-shaped electrodes. In the experiment, the fixed structure keeps this area constant, resulting in a stable induced charge quantity and a constant potential difference between the electrodes; hence, Voc remains at approximately 8.5 V. Isc, however, is directly related to the charge transfer rate. Increasing the rotational speed significantly increases the friction frequency, accelerating the charge transfer rate, and causing the Isc peak to increase from 61 nA to 532 nA. This demonstrates the characteristic that voltage output depends on structural parameters while current output responds dynamically to

changes. Thanks to the excellent properties of the dielectric layer PTFE film, including non-stickiness, high-temperature resistance, and low friction coefficient, the P-TENG has a stable operational foundation. As shown in the durability test data in Table 1, after continuous operation at a speed of 500 rpm for 4 h, the average Voc and average short-circuit current Isc remained relatively stable compared to the initial operating stage, with no significant sharp decline. The overall performance was approximately 92% of the initial state, which fully verifies the durability of P-TENG. For the power output performance of P-TENG, at 200 rpm, the peak power reached 1.71 μW. Although this power level is far below that of traditional power generation systems, in scenarios such as low-power IoT nodes in open farmland or remote sensing devices in remote areas, the output energy, when effectively managed, can meet the operational requirements of certain electronic devices, providing a feasible energy solution for distributed self-powered systems.

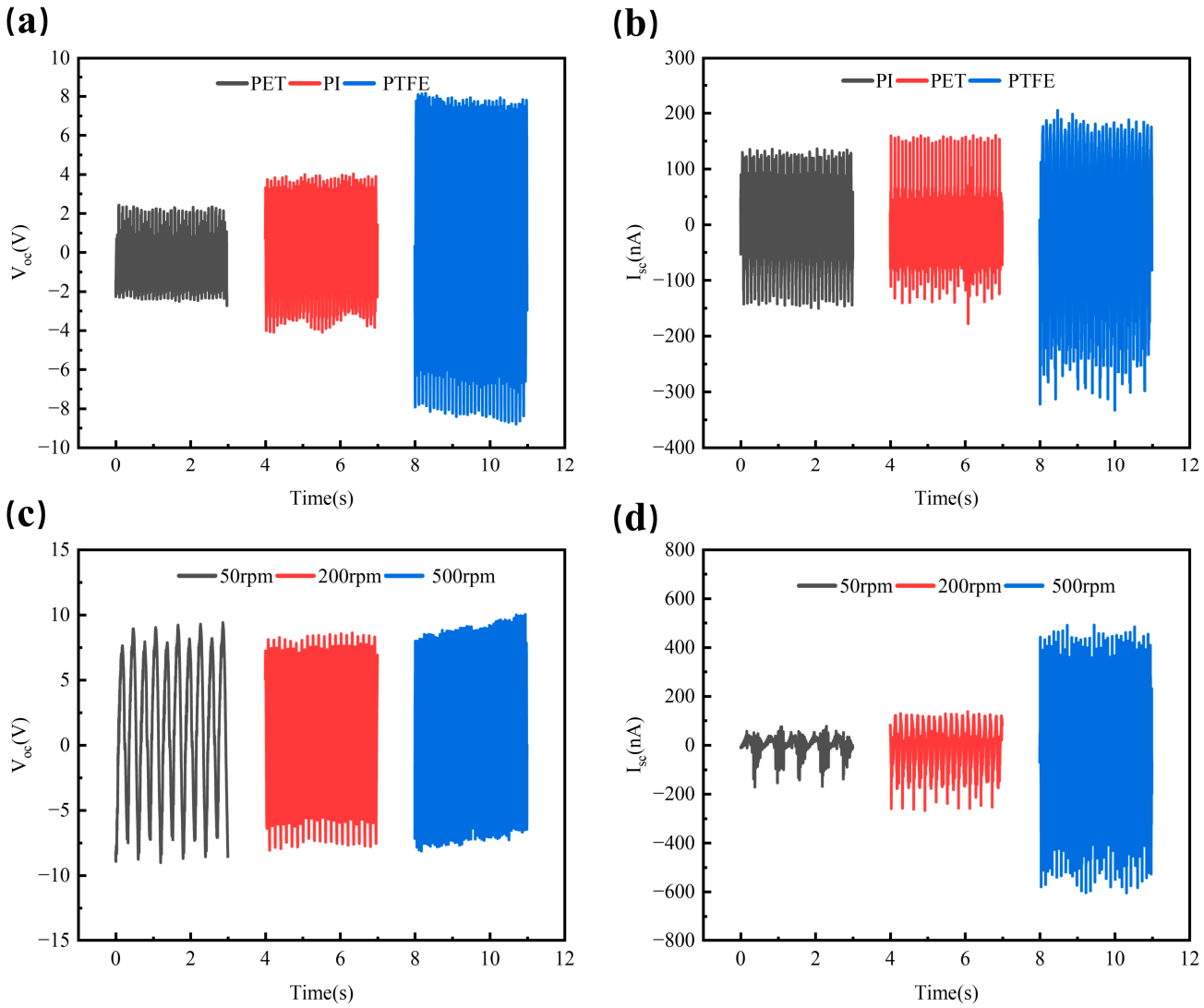


Figure 4. Performance of the P-TENG: (**a**) Open circuit voltage of different dielectric layers. (**b**) Short-circuit current of different dielectric layers. (**c**) Open-circuit voltage at different speeds. (**d**) Short-circuit current at different speeds.

Table 1. Durability performance.

	Peak Average Value 1 Hour Later	Peak Average Value 2 Hours Later	Peak Average Value 3 Hours Later	Peak Average Value 4 Hours Later
V_{oc} (V)	8.35	8.29	8.23	8.16
I_{sc} (nA)	524	513	501	492

Additionally, the number of interdigitated electrodes plays a crucial role in regulating the output performance of P-TENG. We conducted a systematic investigation into the output characteristics under different electrode configurations, with experimental results shown in Table 2. The Voc of P-TENG does not exhibit a significant increasing trend and remains stable at approximately 8 V. This is primarily determined by the core mechanisms, namely, the surface charge density of the friction material and the interlayer spacing of the friction layer, which are weakly correlated with the number of electrodes; while the Isc exhibits a characteristic of first increasing and then stabilizing as the number of electrodes increases. This is because, in the initial stage, the expansion of the total effective area of the electrodes enhances capacitance and its rate of change, while the edge field effect is strengthened, synergistically promoting charge transfer rates and increasing the Isc. However, once the number of electrodes reaches a critical value, the overlapping of edge fields between adjacent electrodes leads to a diminishing return in edge effect gains, and the total charge quantity of the friction layer imposes an upper limit constraint, resulting in a slowing and stabilization of the Isc growth.

Table 2. Output performance of different numbers of electrodes.

	8	**16**	**24**	**32**	**40**	**48**
V_{oc} (V)	7.91	8.13	7.95	8.08	8.23	8.17
I_{sc} (nA)	67	116	147	191	213	202

Using a stepper motor as the excitation source for a simulated seeder, the output characteristics of the EMG were investigated. Figure 5a shows the structural diagram of the EMG section. As shown in the experimental data in Figure 5b,c, the output performance of the EMG is positively correlated with rotational speed. When the rotational speed increases from 30 rpm to 300 rpm, Voc increases from 1 V to 8.7 V, and Isc increases from 45 mA to 294 mA. Similar to P-TENG, durability performance was conducted on the EMG. After continuous operation for 4 h, the EMG performance showed no significant degradation, verifying its excellent stability. To further investigate the performance of the EMG under different load resistances in practical working scenarios, as shown in the results of Figure 5d,e, as the load resistance increases, the load voltage shows an upward trend, while the load current decreases accordingly, providing key performance parameters for optimizing EMG applications. In studies of the EMG's maximum output power, at a rotational speed of 200 rpm, when the load resistance was 31.5 ohms, the maximum peak power reached 110 milliwatts. This substantial power output enables the EMG to rapidly inject electrical energy into microcapacitors of varying capacities. With this efficient charging capability, it can reliably power the sensing system, ensuring continuous and reliable operation of sensor monitoring and data transmission.

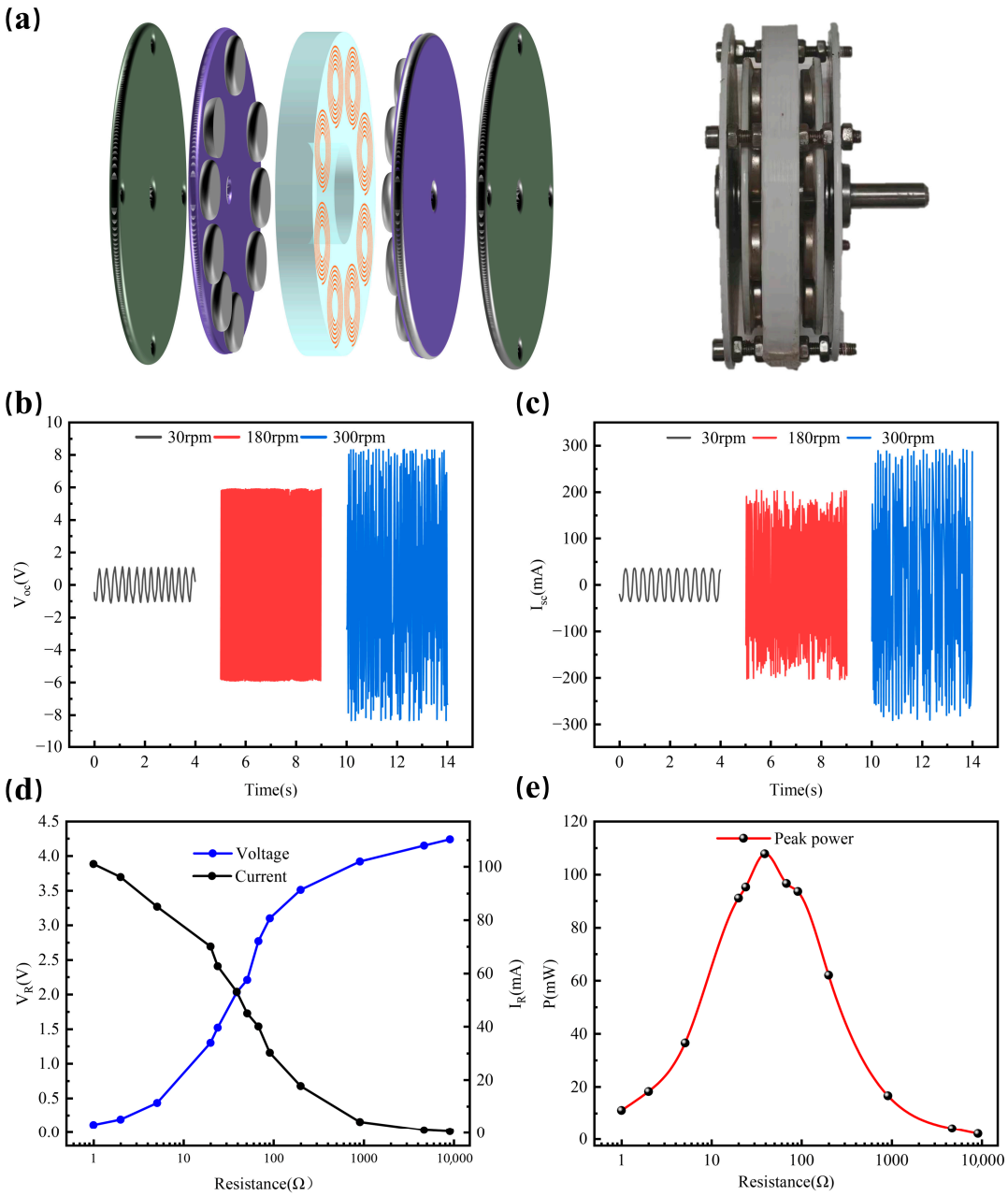


Figure 5. Performance of the EMG: (**a**) Mechanical structure of EMG. (**b**) Open-circuit voltage at different speeds. (**c**) Short-circuit current at different speeds. (**d**) Voltage and current under different loads at a speed of 200 rpm. (**e**) Peak power under different loads.

3.3. System Application Performance

To validate the suitability of the EPTG self-powered wireless sensing system for corn seeding applications, a test system was constructed as shown in Figure 6a. In agricultural mechanization operations, a stable energy supply is the core foundation for the long-term operation of sensing systems [39]. This sensing system uses EPTG as the core self-powered unit. This unit employs a coupled design of P-TENG and EMG, utilizing the mechanical energy generated by the rotation of the seed dispenser during corn seeding machine operations to drive the EPTG, thereby achieving efficient capture and conversion of mechanical energy. The captured energy is processed through a rectification and filtering module for waveform correction and noise filtering, then boosted in voltage via a voltage-boosting module before being directed to charge a 5 V 900 mAh energy storage battery.

This energy storage battery serves as an auxiliary energy storage unit, reducing the impact of instantaneous mechanical energy fluctuations on power supply stability. Based on an energy management strategy, it stores excess energy when mechanical energy is abundant and releases energy when mechanical energy is scarce, establishing a closed-loop system from energy capture and storage to a stable power supply, ensuring the continuity and stability of the system's energy supply. The stable electrical energy output by the energy storage battery powers the IR sensor, TH sensor, and MCU. The IR sensor collects non-contact monitor parameters such as corn seeding spacing and seeding density, while the TH sensor precisely collects environmental temperature and humidity data. The multi-dimensional environmental information collected by both sensors is preliminarily processed by the MCU, then wirelessly transmitted to the cloud platform for visualization analysis. This provides foundational sensory data for subsequent corn seeding decisions, thereby validating the adaptability of the EPTG self-powered wireless sensing system in corn seeding scenarios, from energy supply to information sensing.

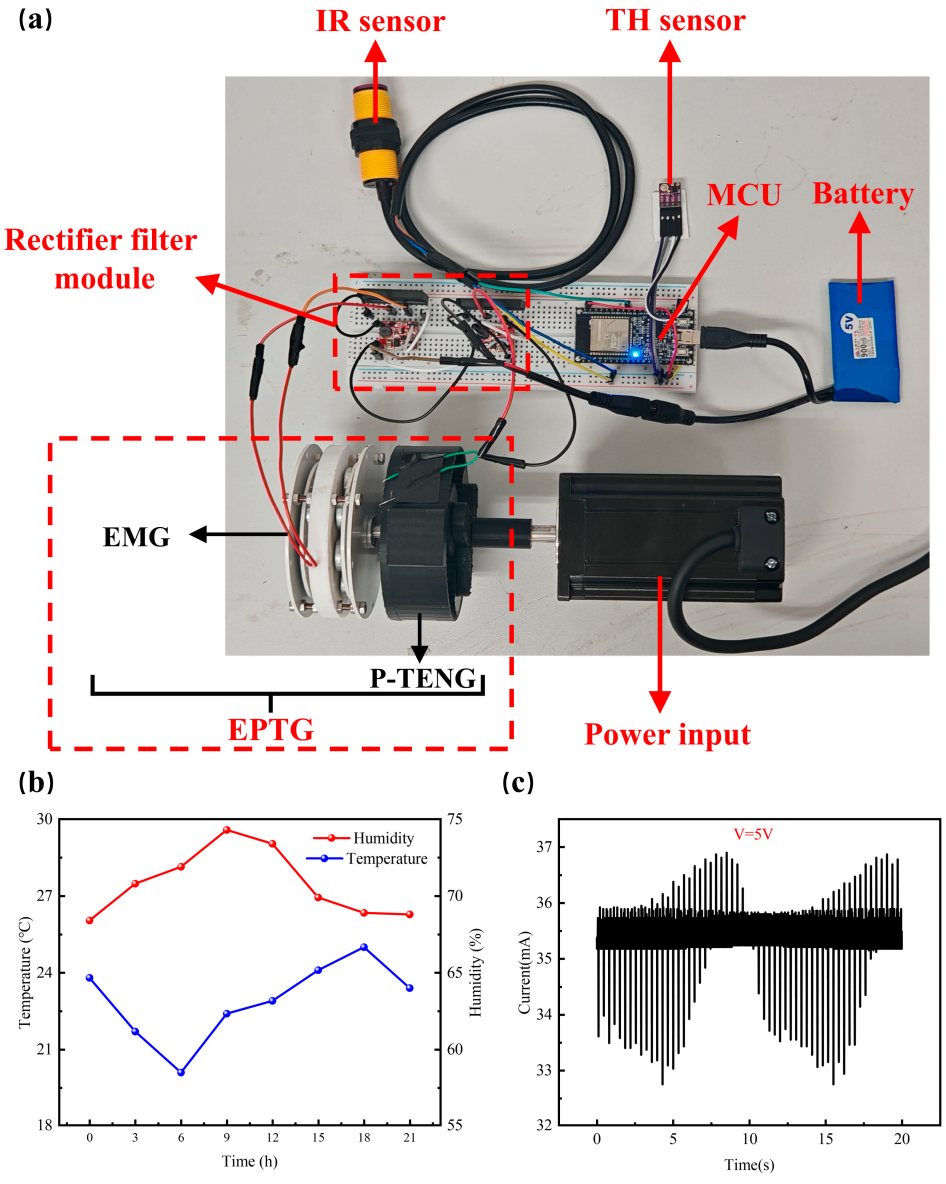


Figure 6. Actual performance of the sensing system: (**a**) Sensing system based on EPTG. (**b**) Actual monitoring data from the TH sensor. (**c**) Power consumption of the sensing system.

(1) EPTG output power

To evaluate the energy supply efficiency of the EPTG self-powered system in corn seeding applications, a test platform for power output monitoring and charging management was constructed. The system is based on an innovative coupling design of P-TENG and EMG, which converts the rotational mechanical energy of the seeder's transmission components into alternating current. After optimization through rectification, filtering, and a boost module, the system conducts output power characteristic tests using an external variable load. Output power tests were conducted under typical operating conditions of a corn seeder (average rotational speed of 25 rpm). To enhance mechanical energy conversion efficiency and meet high-power output requirements, a planetary gear transmission structure was adopted for speed amplification and torque regulation. Through theoretical calculations and experimental verification, the following parameters were selected: 140 teeth for the ring gear, 60 teeth for the planetary gear, and 20 teeth for the sun gear. These parameters effectively enhance the power output of the energy capture components. Test results show that the optimized EPTG system achieves a stable power output of 105 mW under these operating conditions. Through charging mode verification, this power output ensures that a 900 mAh battery receives continuous effective energy replenishment during a typical operating cycle, providing a reliable energy supply for the stable operation of self-powered sensing devices. This fully validates the engineering applicability and energy supply reliability of the EPTG system in agricultural machinery applications.

(2) Power consumption of sensing system

To address the low-speed operation characteristics of corn seeders, the sensing system adopts a low-power strategy combining deep sleep mode with intermittent wake-up. The microcontroller enters a deep sleep mode with microampere-level current consumption during non-operational periods, resulting in extremely low power consumption. It only briefly wakes up during data collection and transmission, as shown in Figure 6c, where the current exhibits periodic fluctuations between 34 and 37 mA, corresponding to an instantaneous power consumption of approximately 170 mW. This strategy significantly reduces the system's average power consumption, keeping it within the coverage range of the EPTG's stable output power of 105 mW. Combined with the energy storage and buffering effect of a 900 mAh battery, this creates a dynamic balance between energy harvesting, energy storage, and low-power consumption, providing reliable energy assurance for the long-term stable operation of the sensing device. This fully validates the effectiveness of this low-power strategy in enhancing the self-powered system of the EPTG.

(3) Data transmission

To assess the reliability of wireless transmission of sensor data in an open field corn seeding scenario, this test verifies the transmission stability and anti-interference performance under different environmental conditions. A high-performance corn seeding sensing system must have a long effective communication distance and strong anti-interference capabilities. The test results are shown in Table 3. In open farmland, the WIFI module and the sensing system achieved an effective communication distance of 60 m, enabling stable transmission of data such as seeding density, spacing, and environmental temperature and humidity. However, when the transmission distance exceeded 60 m, the packet loss rate (PLR) significantly increased, leading to communication interruptions. In densely populated agricultural machinery operation areas, packet loss occurs at 20 m, and transmission stability drops sharply beyond 30 m, making it difficult to ensure the real-time integrity of decision-making data. In actual seeding fields, the density of agricultural machinery equipment is lower than in the densely populated operation areas of the experiment, resulting in weaker signal interference intensity. This reduces interference during sensor

data transmission, improves communication quality, and achieves a more optimal effective transmission distance compared to the experimental scenario [40,41].

Table 3. Communication performance parameters.

	Open Work Area				High-Density Work Area				
Communication distance (m)	10	20	30	60	1	5	10	20	30
Packet loss rate	0	0	0.5%	1.2%	0	0	0	0.4%	2.3%

(4) Sensor module

To validate the collaborative application performance of the designed sensor module in corn seeding operations, an experimental platform was constructed integrating an E18-D80NK infrared reflective photoelectric sensor, an ESP32 main control unit, and an SHT30 temperature and humidity sensor. This platform simulates the dynamic scenario of seeds falling from the seeding tube in a field. As shown in Figure 7, the photoelectric sensor is deployed at the exit of the seed distribution channel. When seeds fall and block the infrared light path, it triggers a change in the signal level, enabling seed detection. The temperature and humidity sensors are installed around the seed dispensing tube to simultaneously collect environmental temperature and humidity data during the operation. The signals collected by both sensors are processed by the MCU and displayed in real time on the upper-level computer cloud platform, showing seeding density, seeding spacing, and environmental temperature and humidity information. A 200 ms anti-vibration mechanism is also set to filter out false triggers caused by equipment vibration or repeated seed obstruction.



Figure 7. Actual test of corn seed drop using an IR sensor.

To verify the recognition accuracy of the IR photoelectric sensor in corn seeding operations, the experimental platform used 200 uniformly sized, intact corn seeds per group as standard samples and conducted three independent trials. The results showed that the photoelectric sensor recognized 185, 192, and 187 seeds, respectively, with an average recognition accuracy of 94%. This result indicates that the photoelectric sensor can accurately identify the seed drop situation of corn seeds, providing reliable data support for seeding monitoring.

The performance of temperature and humidity sensors involves comparing the collected data with standard equipment to verify accuracy, with deviation values falling within the permissible range. As shown in Figure 6b, the system can stably collect temperature and humidity data throughout the day. It is worth noting that temperature and

humidity sensors not only monitor the sowing environment in real time but also provide critical evidence for analyzing the impact of environmental conditions on sowing quality: high humidity may cause water vapor to adhere to the seed surface, interfering with the blocking effect of the infrared light path; and temperature changes may alter the physical properties of seeds (such as hardness and elasticity), thereby affecting their falling posture and speed in the seed dispensing channel. By synchronously collecting seed dispensing data and temperature and humidity parameters, this lays the foundation for subsequent development of accuracy compensation models and optimization of seeding operation parameters.

In summary, this sensing system achieves precise monitoring of the seed falling process and simultaneous acquisition of environmental temperature and humidity data, providing technical support for intelligent sowing monitoring and creating conditions for environmental adaptability analysis. It has certain application value in the field of agricultural intelligent equipment.

4. Conclusions

This study proposes a self-powered sensing system based on a planetary gear-coupled triboelectric nanogenerator (P-TENG) and an electromagnetic generator (EMG). The system utilizes the speed gain characteristics of planetary gears and flexibly designs gear ratios to adapt to various operating conditions, providing stable energy input to the composite power generation unit and significantly improving mechanical energy capture and conversion efficiency. The application of the EPTG module reduces the reliance of corn seeding monitoring equipment on external power sources and enhances adaptability to complex agricultural environments. Experimental results show that the system stably outputs 105 mW of power at a seeder speed of 2 rpm. When combined with a power management module, it can continuously charge a 5 V 900 mAh energy storage battery, with long-term durability test performance retention rates reaching 92%. The system's low-power program design enables stable operation of the integrated IR sensor and TH sensor unit in self-powered mode. The IR sensor achieves a monitoring accuracy of 94% for seed drop success rates, and sensor data can be wirelessly transmitted to the host computer within a 50 m range in open fields. The cloud platform performs real-time visualization analysis, providing decision support for precise seeding. The system integrates composite energy harvesting and intelligent sensing technologies to provide a feasible solution for energy self-sufficiency and precision operations in agricultural smart equipment. The flexible design of the planetary gears further highlights its application potential in diverse agricultural scenarios.

Author Contributions: Conceptualization, L.M. and H.W.; Methodology, L.M., H.W. and Z.Y.; Software, D.W. and M.Y.; Formal analysis, L.M., H.W.; Investigation, R.Z. and Z.Y.; Resources, L.M. and H.W.; Data curation, L.M. and H.W.; Writing—original draft, L.M.; Writing—review & editing, L.M.; Supervision, X.X.; Funding acquisition, X.X. All authors have read and agreed to the published version of the manuscript.

Funding: This research received no external funding.

Data Availability Statement: Data are contained within the article.

Conflicts of Interest: The authors declare no conflict of interest.

References

1. Erenstein, O.; Chamberlin, J.; Sonder, K. Estimating the global number and distribution of maize and wheat farms. *Glob. Food Secur.* **2021**, *30*, 100558. [CrossRef]
2. Guzzon, F.; Arandia Rios, L.W.; Caviedes Cepeda, G.M.; Céspedes Polo, M.; Chavez Cabrera, A.; Muriel Figueroa, J.; Medina Hoyos, A.E.; Jara Calvo, T.W.; Molnar, T.L.; Narro León, L.A. Conservation and use of Latin American maize diversity: Pillar of nutrition security and cultural heritage of humanity. *Agronomy* **2021**, *11*, 172. [CrossRef]
3. Tu, K.; Wen, S.; Cheng, Y.; Zhang, T.; Pan, T.; Wang, J.; Wang, J.; Sun, Q. A non-destructive and highly efficient model for detecting the genuineness of maize variety 'JINGKE 968' using machine vision combined with deep learning. *Comput. Electron. Agric.* **2021**, *182*, 106002. [CrossRef]
4. Cay, A.; Kocabiyik, H.; May, S. Development of an electro-mechanic control system for seed-metering unit of single seed corn planters Part I: Design and laboratory simulation. *Comput. Electron. Agric.* **2018**, *144*, 71–79. [CrossRef]
5. Khernane, S.; Bouam, S.; Arar, C. Renewable energy harvesting for wireless sensor networks in precision agriculture. *Int. J. Networked Distrib. Comput.* **2024**, *12*, 8–16. [CrossRef]
6. Sajib, M.M.H.; Sayem, A.S.M. Innovations in Sensor-Based Systems and Sustainable Energy Solutions for Smart Agriculture: A Review. *Encyclopedia* **2025**, *5*, 67. [CrossRef]
7. Xu, N.; Han, J.; Xiong, Y.; Wang, Z.L.; Sun, Q. TENG applications in transportation and surrounding emergency management. *Adv. Sustain. Syst.* **2022**, *6*, 2200267. [CrossRef]
8. Dan, X.; Cao, X.; Wang, Y.; Yang, J.; Wang, Z.L.; Sun, Q. A stereoscopically structured triboelectric nanogenerator for bending sensors and hierarchical interactive systems. *ACS Appl. Nano Mater.* **2023**, *6*, 3590–3598. [CrossRef]
9. Jiao, H.; Lin, X.; Xiong, Y.; Han, J.; Liu, Y.; Yang, J.; Wu, S.; Jiang, T.; Wang, Z.L.; Sun, Q. Thermal insulating textile based triboelectric nanogenerator for outdoor wearable sensing and interaction. *Nano Energy* **2024**, *120*, 109134. [CrossRef]
10. He, L.; Zhang, C.; Zhang, B.; Yang, O.U.; Yuan, W.; Zhou, L.; Zhao, Z.; Wu, Z.; Wang, J.; Wang, Z.L. A dual-mode triboelectric nanogenerator for wind energy harvesting and self-powered wind speed monitoring. *ACS Nano* **2022**, *16*, 6244–6254. [CrossRef]
11. Fan, F.; Tian, Z.; Wang, Z.L. Flexible triboelectric generator. *Nano Energy* **2012**, *1*, 328–334. [CrossRef]
12. Yi, F.; Lin, L.; Niu, S.; Yang, P.K.; Wang, Z.; Chen, J.; Zhou, Y.; Zi, Y.; Wang, J.; Liao, Q. Stretchable-rubber-based triboelectric nanogenerator and its application as self-powered body motion sensors. *Adv. Funct. Mater.* **2015**, *25*, 3688–3696. [CrossRef]
13. Jin, L.; Tao, J.; Bao, R.; Sun, L.; Pan, C. Self-powered real-time movement monitoring sensor using triboelectric nanogenerator technology. *Sci. Rep.* **2017**, *7*, 10521. [CrossRef]
14. Zi, Y.; Guo, H.; Wen, Z.; Yeh, M.; Hu, C.; Wang, Z.L. Harvesting low-frequency (<5 Hz) irregular mechanical energy: A possible killer application of triboelectric nanogenerator. *ACS Nano* **2016**, *10*, 4797–4805. [CrossRef]
15. Li, Z.; Jiang, X.; Xu, W.; Gong, Y.; Peng, Y.; Zhong, S.; Xie, S. Performance comparison of electromagnetic generators based on different circular magnet arrangements. *Energy* **2022**, *258*, 124759. [CrossRef]
16. Zhang, B.; Zhang, S.; Li, W.; Gao, Q.; Zhao, D.; Wang, Z.L.; Cheng, T. Self-powered sensing for smart agriculture by electromagnetic–triboelectric hybrid generator. *ACS Nano* **2021**, *15*, 20278–20286. [CrossRef] [PubMed]
17. Zhao, B.; Li, Z.; Liao, X.; Qiao, L.; Li, Y.; Dong, S.; Zhang, Z.; Zhang, B. A heaving point absorber-based ocean wave energy convertor hybridizing a multilayered soft-brush cylindrical triboelectric generator and an electromagnetic generator. *Nano Energy* **2021**, *89*, 106381. [CrossRef]
18. Chen, J.; Wu, K.; Gong, S.; Wang, J.; Wang, K.; Guo, H. A magnetic-multiplier-enabled hybrid generator with frequency division operation and high energy utilization efficiency. *Research* **2023**, *6*, 168. [CrossRef]
19. Xing, F.; Tang, G.; Wang, H.; Wang, M.; Wu, M.; Xu, M. Exploring the Synergy of EMG and TENG in Motion Based Hybrid Energy Harvesting. *Nano Energy* **2024**, 110584. [CrossRef]
20. Zhang, T.; Yang, T.; Zhang, M.; Bowen, C.R.; Yang, Y. Recent progress in hybridized nanogenerators for energy scavenging. *Iscience* **2020**, *23*, 101689. [CrossRef] [PubMed]
21. Lee, J.; Heo, D.; Lyu, H.; Hur, J.W.; Kim, S.; Lin, Z.; Park, J.Y.; Lee, S. Slinky-inspired triboelectric–electromagnetic hybrid generator. *Curr. Appl. Phys.* **2023**, *49*, 109–114. [CrossRef]
22. Zeeshan Ahmed, R.; Chun, W.; Oh, S.J.; Kim, Y. Power generation from a hybrid generator (TENG-EMG) run by a thermomagnetic engine harnessing low temperature waste heat. *Energies* **2019**, *12*, 1774. [CrossRef]
23. Bjelica, J.M.; Djuric, N.M.; Djuric, S.M. Performance analysis and application of a hybrid electromagnetic-triboelectric nanogenerator for energy harvesting. *Energy Rep.* **2022**, *8*, 9184–9200. [CrossRef]
24. Niu, S.; Xu, H.; Sun, Z.; Shao, Z.Y.; Jian, L. The state-of-the-arts of wireless electric vehicle charging via magnetic resonance: Principles, standards and core technologies. *Renew. Sustain. Energy Rev.* **2019**, *114*, 109302. [CrossRef]
25. Nia, A.R.; Awasthi, A.; Bhuiyan, N. Industry 4.0 and demand forecasting of the energy supply chain: A literature review. *Comput. Ind. Eng.* **2021**, *154*, 107128. [CrossRef]
26. Meng, Y.; Wu, C.; Ling, L. Mathematical modeling of the transmission performance of 2K–H pin cycloid planetary mechanism. *Mech. Mach. Theory* **2007**, *42*, 776–790. [CrossRef]

27. Wang, C. High power density design for planetary gear transmission system. *Proc. Inst. Mech. Eng. Part C J. Mech. Eng. Sci.* **2019**, *233*, 5647–5658. [CrossRef]
28. Qian, P.; Zhang, Y.; Cheng, G.; Ge, S.; Zhou, C. Model analysis and verification of 2K–H planetary gear system. *J. Vib. Control.* **2015**, *21*, 1946–1957. [CrossRef]
29. Albalawi, H.; Eisa, A. Bankruptcy problem in energy warehouse: Applications and challenges. *Ain Shams Eng. J.* **2023**, *14*, 102011. [CrossRef]
30. Roy, S.; Kabir, M.H.; Salauddin, M.; Halim, M.A. An electromagnetic wind energy harvester based on rotational magnet pole-pairs for autonomous IoT applications. *Energies* **2022**, *15*, 5725. [CrossRef]
31. Zhu, J.; Zhu, M.; Shi, Q.; Wen, F.; Liu, L.; Dong, B.; Haroun, A.; Yang, Y.; Vachon, P.; Guo, X. Progress in TENG technology—A journey from energy harvesting to nanoenergy and nanosystem. *EcoMat* **2020**, *2*, e12058. [CrossRef]
32. Luo, J.; Wang, Z.L. Recent progress of triboelectric nanogenerators: From fundamental theory to practical applications. *EcoMat* **2020**, *2*, e12059. [CrossRef]
33. Wu, Z.; Chen, X.; Wan, Z.; Chi, J.; Zhang, R.; Wang, M.; Song, D.; Xiao, X. Self-powered wireless flexible sensing for food storage based on triboelectric-electromagnetic generator. *Mater. Today Sustain.* **2024**, *26*, 100781. [CrossRef]
34. Zhao, S.; Han, G.; Deng, H.; Ma, M.; Zhong, X. Research on the Sensing Characteristics of an Integrated Grid-like Sensor Based on a Triboelectric Nanogenerator. *Sensors* **2024**, *24*, 869. [CrossRef]
35. Gomes, A.; Rodrigues, C.; Pereira, A.M.; Ventura, J. Influence of thickness and contact area on the performance of PDMS-based triboelectric nanogenerators. *arXiv* **2018**, arXiv:1803.10070.
36. Chen, J.; Wei, X.; Wang, B.; Li, R.; Sun, Y.; Peng, Y.; Wu, Z.; Wang, P.; Wang, Z.L. Design optimization of soft-contact freestanding rotary triboelectric nanogenerator for high-output performance. *Adv. Energy Mater.* **2021**, *11*, 2102106. [CrossRef]
37. Cao, X.; Zhou, H.; Zhou, Y.; Hu, Y.; Wang, Y.; Wang, Z.L.; Sun, Q. High performance rotary-structured triboelectric-electromagnetic hybrid nanogenerator for ocean wind energy harvesting. *Adv. Mater. Technol.* **2023**, *8*, 2300327. [CrossRef]
38. Wang, Y.; Wang, N.; Cao, X. From Triboelectric Nanogenerator to Hybrid Energy Harvesters: A Review on the Integration Strategy toward High Efficiency and Multifunctionality. *Materials* **2023**, *16*, 6405. [CrossRef]
39. Luo, H.; Yang, T.; Jing, X.; Cui, Y.; Qin, W. Environmental energy harvesting boosts self-powered sensing. *Mater. Today Energy* **2024**, *40*, 101502. [CrossRef]
40. Rao, Y.; Xu, W.; Zhu, J.; Jiang, Z.; Wang, R.; Li, S. Practical deployment of an in-field wireless sensor network in date palm orchard. *Int. J. Distrib. Sens. Netw.* **2017**, *13*, 468701065. [CrossRef]
41. Roccia, C.; Teruel, B.; Alves, E.C.D.S.; Arnold, F.; Bravo-Roger, L.; Moretti, A.; Gonçalves, M.S. Experimental evaluation of the performance of a wireless sensor network in agricultural environments. *Eng. Agrícola* **2012**, *32*, 1165–1175. [CrossRef]

Disclaimer/Publisher's Note: The statements, opinions and data contained in all publications are solely those of the individual author(s) and contributor(s) and not of MDPI and/or the editor(s). MDPI and/or the editor(s) disclaim responsibility for any injury to people or property resulting from any ideas, methods, instructions or products referred to in the content.